

RPA: a Simple, Efficient and Flexible Policy for Input Buffered Switches

*Original*

RPA: a Simple, Efficient and Flexible Policy for Input Buffered Switches / AJMONE MARSAN, Marco Giuseppe; Bianco, Andrea; Leonardi, Emilio. - In: IEEE COMMUNICATIONS LETTERS. - ISSN 1089-7798. - 1:(1997), pp. 83-86.

*Availability:*

This version is available at: 11583/1401850 since:

*Publisher:*

IEEE

*Published*

DOI:

*Terms of use:*

This article is made available under terms and conditions as specified in the corresponding bibliographic description in the repository

*Publisher copyright*

(Article begins on next page)

# PROGRESS TOWARDS HIGH EFFICIENCY THIN-FILM III-V QUANTUM DOT SOLAR CELLS FOR SPACE

T. Aho<sup>(1)</sup>, A. Tukiainen<sup>(1)</sup>, F. Elsehrawy<sup>(2)</sup>, A. Khalili<sup>(2)</sup>, J. Lyytikäinen<sup>(1)</sup>, E. Halonen<sup>(1)</sup>,  
T. Niemi<sup>(1)</sup>, M. Guina<sup>(1)</sup>, F. Cappelluti<sup>(2)</sup>

<sup>(1)</sup> Optoelectronics Research Centre, Laboratory of Photonics, Tampere University of Technology,  
P.O. Box 527, FI-33101 Tampere, Finland. Email: mircea.guina@tut.fi

<sup>(2)</sup> Department of Electronics and Telecommunications, Politecnico di Torino  
Corso Duca degli Abruzzi 24, 10129, Torino, Italy. Email: federica.cappelluti@polito.it

**ABSTRACT:** This work summarizes our results in the development of high efficiency III-V quantum dot (QD) solar cells, aimed at tackling with two of the most relevant issues posed by QD solar cells (QDSCs), namely the degradation of open circuit voltage and the weak photon harvesting by QDs. In particular, we report our latest achievements in: i) The molecular beam epitaxy growth of high-quality QDSCs, demonstrating  $V_{oc}$  as high as 0.94 V and low penalty ( $\sim 40$  mV) with respect to the single-junction reference cell. ii) The development by nanoimprint lithography of metal/polymer back reflectors with high diffraction efficiency, enabling four times increase of the QD photogenerated current. Experimental results are discussed with the support of numerical simulations.

**Keywords:** III-V semiconductors; Quantum Dots; Light Trapping; Thin Film

## 1 INTRODUCTION

Future applications in space and aeronautics demand for very high efficiency, lightweight and flexible solar cells. To achieve these goals, several approaches are investigated worldwide to bring new concepts in the consolidated III-V single- and multi-junction solar cells, such as thin-film architectures, novel materials, nanostructures, and nanophotonics. The successful exploitation of these concepts may bring cost-effective and attractive options for next generation space solar cells. In particular, QDs have potential impact on diverse aspects of space photovoltaics, such as improved current matching in multijunction cells by bandgap tuning [1] and enhanced radiation hardness [2]. However, a number of issues need to be solved in order to achieve high efficiency QD-based solar cells.

In [3] we have shown through electrical simulations that the bandgap-voltage offset of QD solar cells (QDSC) operating in the thermal limit [4], i.e. with carriers undergoing full thermalization, is expected to be comparable to that one of III-V single-junction cells. In fact, the large degradation of the open circuit voltage ( $V_{oc}$ ) often observed in experiments is due to extrinsic loss caused by material quality issues. Of the same signature were the conclusions drawn in [5, 6] based on detailed balance arguments. Therefore, material optimization is a key task to demonstrate high-efficiency QDSCs. Moreover, the absorptivity of the solar cell must be substantially increased by suitable photon management approaches. In [3] we demonstrated doubled QD photocurrent by substrate removal through epitaxial lift-off and integration of a rear planar reflector. Much higher enhancement of the QD current is expected by implementing diffraction gratings within such thin-film architecture.

## 2 METHODS

### 2.1 Solar cell fabrication and characterization

The InAs/GaAs QD samples and solar cells were grown on p-GaAs(100) substrates using a V90 molecular beam epitaxy (MBE) system. The GaAs-based layers were grown at 580 °C. Growth temperatures for InAs QDs and AlInP were 465-475 °C and  $\sim 490$  °C, respectively. Thin GaAsP strain-balancing layers were

also grown within the undoped GaAs barrier layers between the QD sheets.

6×6 mm<sup>2</sup> solar cells were fabricated by dicing and using a shadow mask process for the front-side grid metal deposition in an electron beam evaporator. No anti-reflection coating was deposited onto the cells. The electrical parameters of the solar cells were determined using light-biased current-voltage (I-V) and external quantum efficiency (EQE) measurements.

### 2.2 Gratings fabrication and characterization

Grating prototypes were fabricated on double-side polished 350  $\mu\text{m}$  semi-insulating GaAs wafer by nanoimprint lithography (NIL). Being the substrate almost transparent at the QD wavelengths it provides a suitable platform to test the diffraction properties of the grating. The grating is patterned onto a commercial OrmoComp NIL photoresist by using an in-house fabricated Si master. In order to achieve the desired grating dimensions, the master was realized by a sequential optimized processing involving a first patterning step by electron beam lithography into a sacrificial Si wafer and a second one by NIL and dry etching onto the final Si master. From the master, the grating was then transferred to polydimethylsiloxane stamp and finally imprinted to the NIL photoresist. 200 nm Ag was deposited on top of the polymer layer using electron beam evaporator. The fabricated grating has height of 700 nm and period of 2.5  $\mu\text{m}$ , according to numerical optimization aimed at maximizing the diffraction efficiency at the QD wavelengths [7].

The grating morphology was characterized with a scanning electron microscope (SEM). Specular and total reflectance were measured with a PerkinElmer Lambda 1050 spectrophotometer which includes an integrating sphere module. To quantify the amount of the diffracted light, a variable angle measurement technique has been used, where the sample is illuminated with incident angle of 8°, and the diffracted light is collected at variable angles from 8° to 48° with an optical fiber connected to a spectrometer. This allows to quantify the grating diffraction efficiency as the ratio between the collected diffracted power and the incident power. For the grating under study this allowed to analyze diffraction orders of  $m=0$  and  $m=\pm 1$ .

### 2.3 Modeling

The solar cells were simulated using a drift-diffusion

Poisson model coupled with a rate-equation model for the carrier processes involving the QD states (see the QD electronic structure in Fig.1) and charge transfer between QD states and the continuum bands. Such an approach allows for an accurate and detailed analysis of the solar cell physics and it is developed to be thermodynamic consistent [3, 8].

The grating structures were simulated using the rigorous coupled-wave analysis (RCWA) method with

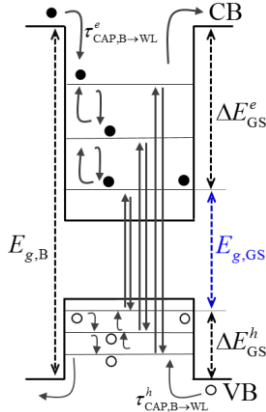


**Figure 1:** QD electronic structure with the indication of the carrier processes involved in thermally-limited QDSCs.  $E_{g,B}$ ,  $E_{g,GS}$  are the GaAs and GS bandgap energy, respectively.

the RSoft DiffractMOD software (Synopsys). Material optical models are derived from the literature or –in the case of the QD stack – from optical or electro-optical characterization. In particular, the reported case study assumes a QD absorption coefficient estimated from the EQE measurement of a previous generation of fabricated QDSCs [3]. The absorbance spectrum was estimated from the absorbed photon density in the photoactive region only, and thus does not include absorption in the contact and metal layers. The corresponding QD photocurrent density can be estimated by integrating the absorbance over the solar spectrum of interest in the 895 nm – 1200 nm range.

### 3 RESULTS AND DISCUSSION

QDSCs with deep-junction (DJ) and shallow-junction (SJ) configuration were designed and fabricated. As shown in Fig.2, in both cases, the multi-layer QD stack is placed in an intrinsic GaAs region next to the emitter-base junction. The QD placement in the high field region ensures full carrier collection at short circuit. Fig.3 shows the calculated  $V_{oc}$  for QD cells with nominal ground state (GS) emission at 1033 nm ( $E_{g,GS} = 1.2$  eV) and different arrangements of the QD stack as a function of the QD in-plane density. Assuming realistic non radiative recombination loss in the GaAs interdot layers (SRH lifetime  $\sim 50$  ns),  $V_{oc}$  higher than 0.9 V is predicted. Non radiative recombination is minimized by shrinking the intrinsic region, provided that the material quality remains high. The achievable open circuit voltage decreases as the number of layers increase due to the increased radiative recombination through the QD states.

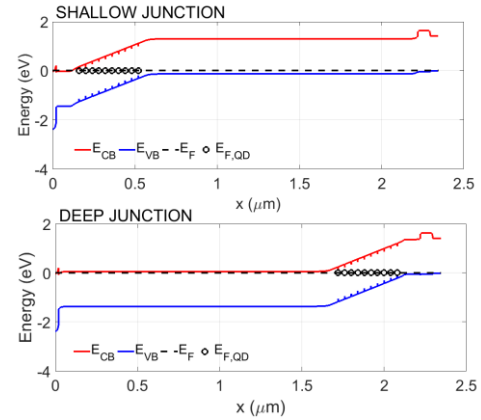
Several solar cells with 10 and 20 QD layers– both with DJ and SJ configuration - were grown by MBE exploiting thin GaAsP strain balancing layers in the

GaAs interdot layers. The QD in-plane density was estimated to be about  $7 \times 10^{10}$  cm<sup>-2</sup>. Depending on the device configuration, QDs showed photoluminescence (PL) peak between 1015 nm and 1040 nm, and wetting layer emission around 920 nm. More details about material characterization and External Quantum Efficiency measurements were reported in [9].

Both DJ and SJ QDSCs showed only 40 mV  $V_{oc}$  penalty with respect to their GaAs reference, comparable to that one reported by Bailey et al. [1] with metalorganic vapour phase epitaxy (MOCVD) growth. The highest  $V_{oc}$  (0.94 V) was obtained for the SJ structure, which exhibited a fill factor of about 84 %. On the other hand, DJ cells suffered from slightly higher recombination in the thick emitter.

Shallow junction		Deep junction	
	h [nm]		h [nm]
n-GaAs contact	300	n-GaAs contact	300
n-AlInP window	20	n-AlInP window	20
n-GaAs	100	n-GaAs	1660
InAs QD layers	440	InAs QD layers	440
p-GaAs base	1660	p-GaAs	100
p-Al <sub>0.2</sub> Ga <sub>0.8</sub> As BSF	75	p-Al <sub>0.2</sub> Ga <sub>0.8</sub> As BSF	75
p-GaAs contact	50	p-GaAs contact	50
2" GaAs wafer, p+		2" GaAs wafer, p+	

(a)



(b)

**Figure 2:** (a) Schematic structure of the shallow and deep junction QD cells. (b) Corresponding energy band diagram at thermal equilibrium.

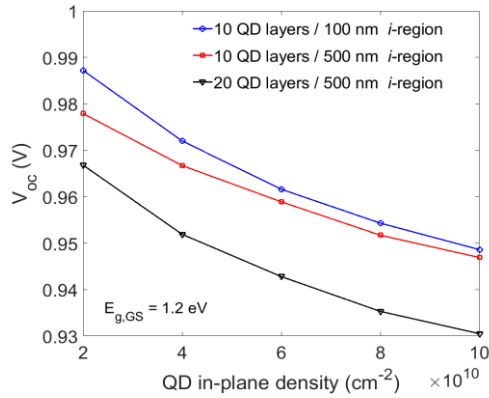


**Figure 3:** Calculated  $V_{oc}$  as a function of the QD in-plane density for different configurations of the QD stack (number of layers and interdot spacing) for QDs with PL peak emission at 1033 nm.

The measured  $V_{oc}$  vs. PL emission wavelength for a wide set of fabricated samples is reported in Fig.4: as expected, the  $V_{oc}$  decreases with the PL wavelength, i.e. with larger QD confinement. The measured values are in line with those expected from the GS transition energy ( $V_{oc}=E_{g,GS}/q-W_{oc}$ ) [10], using for the bandgap-voltage offset ( $W_{oc}$ ) reference values for state-of-art thin-film ( $W_{oc}=0.3$  V) and wafer-based ( $W_{oc}=0.4$  V) GaAs single-gap cells. A  $V_{oc}$  - bandgap offset of 0.3 V was also reported in [11] for a collection of experimental data of high-quality QDSCs. The graph also shows the bandgap-voltage offset as predicted under radiative limited conditions by the QD-corrected drift-diffusion model for a representative case of a 20 layers QDSC. Overall, the presented results demonstrate a high material quality of the fabricated devices.

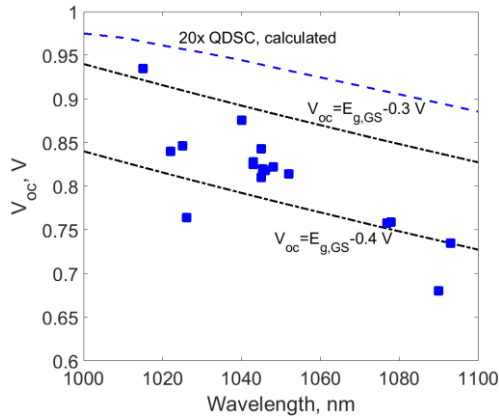


**Figure 4:** Experimental  $V_{oc}$  values of several InAs QDSCs as a function of the PL peak emission wavelength. The black dashed lines indicate reference trends in terms of bandgap voltage offset in state-of-art III-V solar cells [10]. The blue dashed line indicates the scaling law predicted by the QDSC physics-based model.

Light-trapping enhancement of the QD photocurrent may be pursued through a thin-film structure implementing a textured reflector in the rear side of the cell. The absorbance spectra reported in Fig.6 for different configurations of the backside textured

reflector highlight the remarkable absorption increase at the QD wavelengths: the achievable increase of the QD current with respect to a wafer-based configuration ranges from 4 to 7 depending on the material used for the grating fabrication: polymer (low index case study,  $n=1.5$ ) or AlInP (high index case study).

Different geometries and materials have been investigated and described in [12]. Fig.6 summarizes the results of the fabrication of pyramidal metal/polymer back reflectors. Experiments and RCWA simulations demonstrate high diffuse reflectance (Fig. 6 (b)) and efficient diffraction of light (Fig.6 (c)) in the QD wavelength range.

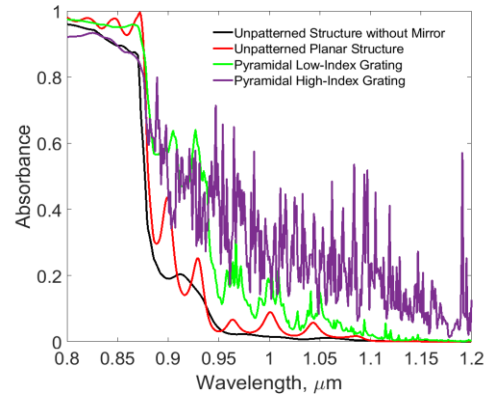


**Figure 5:** Calculated absorbance spectra for a representative 20 layer QDSC with different photonic configurations. The corresponding enhancement of the short circuit current contribution from the QDs with respect to the wafer-based configuration is 1.6, 4, and 7 for the planar reflector, low index pyramid grating and high index pyramid grating, respectively.

#### 4 CONCLUSION

In conclusion, QDSCs with the highest  $V_{oc}$  ever reported for MBE grown QDs and  $V_{oc}$  penalty in line with the state-of-art [2, 3] are demonstrated. Both DJ and SJ configurations show promising performance, enabling cell optimization for highest efficiency at beginning of life or for highest radiation hardness. Fabricated metal/polymer photonic gratings demonstrate significant potential for enhancing the QD current contribution. Numerical simulations [4] show that the presented advancements in the technology of QD growth and structures for photon management pave the way to the realization of thin InAs/GaAs QDSCs with target efficiency of 30% - AM1.5G (26% - AM0). The present study – regardless of the specific material system – is also of interest for intermediate band solar cells in concentrator photovoltaics [13]. Finally, the photonic gratings proposed in this work show promising performance and would be suitable for other photovoltaic technologies by proper optimization of the grating geometrical features to match the wavelength range of interest.

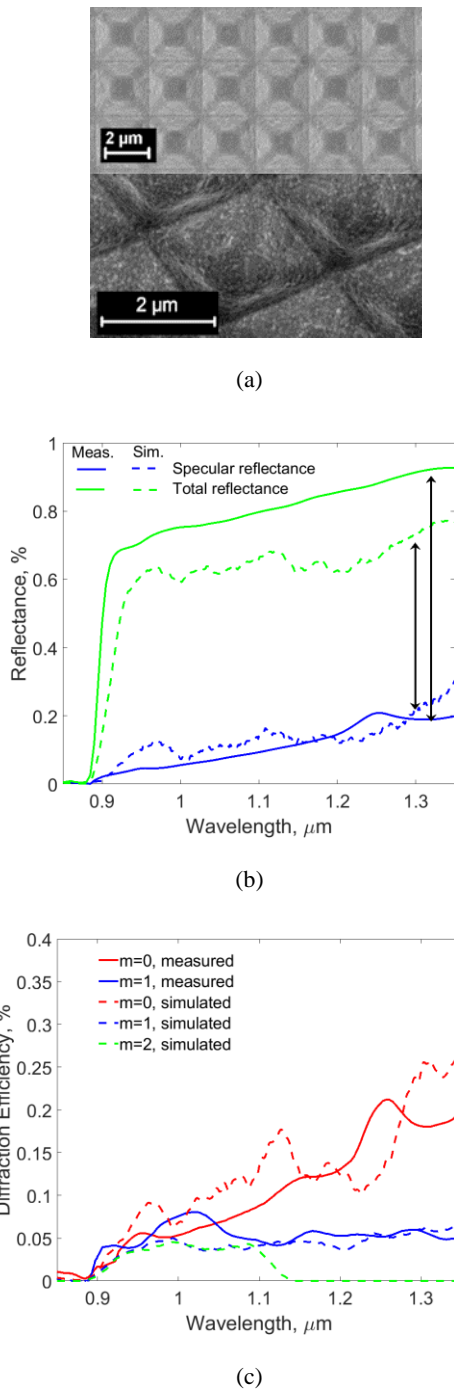


**Figure 6:** (a) SEM image of the pyramid grating. (b) Measured and simulated reflectance. The difference between the total and the specular reflectance represents the amount of diffuse light (the black double-headed arrows). In contrast, planar structures – not shown here – demonstrated marginal difference between total and specular reflectance. (c) Measured and simulated diffraction efficiency.

#### Acknowledgements

The work was partly funded by European Union Horizon 2020 project TFQD (Grant Agreement No. 687253) and ERC AdG project AMETIST (Grant Agreement No. ERC-2015-AdG 695116).

#### 4.3 References

- [1] C.G. Bailey, D.V. Forbes, R.P. Raffaele, S.M. Hubbard, "Near 1 V open circuit voltage InAs/GaAs quantum dot solar cells," *Appl. Phys. Lett.* 98 (16) (2011) 163105.
- [2] C.D. Cress et al, "Quantum dot solar cell tolerance to alpha-particle irradiation," *Appl. Phys. Lett.*, 91.18 (2007): 183108.
- [3] F. Cappelluti, D. Kim, M. van Eerden, A. P. Cédola, T. Aho, G. Bissels, F. Elsehrawy, J. Wu, H. Liu, P. Mulder, G. J. Bauhuis, J. J. Schermer, T. Niemi, and M. Guina, "Light-trapping enhanced thin-film III-V quantum dot solar cells fabricated by epitaxial lift-off," *Sol. Energy Mater. Sol. Cells*, <https://doi.org/10.1016/j.solmat.2017.12.014> (2018).
- [4] V. Aroutiounian, S. Petrosyan, A. Khachatryan, K. Touryan, "Quantum dot solar cells," *J. Appl. Phys.* 89 (4) (2001) 2268–2271.
- [5] Yamaguchi, M., Lee, K. H., Araki, K., Kojima, N., Yamada, H., & Katsumata, Y. (2018). Analysis for efficiency potential of high-efficiency and next-generation solar cells. *Progress in Photovoltaics: Research and Applications*, 26(8), 543-552.
- [6] Zhu, L., Akiyama, H., & Kanemitsu, Y. (2018). Intrinsic and extrinsic drops in open-circuit voltage and conversion efficiency in solar cells with quantum dots embedded in host materials. *Scientific reports*, 8(1), 11704.
- [7] A. Musu, F. Cappelluti, T. Aho, V. Polojärvi, T. Niemi, and M. Guina, "Nanostructures for light management in thin-film GaAs quantum dot solar cells," in *Light, Energy and the Environment*, (Optical Society of America, 2016), paper JW4A-45
- [8] A. P. Cédola, D. Kim, A. Tibaldi, M. Tang, A. Khalili, J. Wu, H. Liu, F. Cappelluti, "Physics-Based Modeling and Experimental Study of Si-Doped InAs/GaAs Quantum Dot Solar Cells." *International Journal of Photoenergy* (2018).
- [9] A. Tukiainen, J. Lyytikäinen, T. Aho, E. Halonen, M. Raappana, F. Cappelluti, M. Guina, Comparison of 'shallow' and 'deep' junction architectures for MBE-grown InAs/GaAs quantum dot solar cells. 2018 WCPEC-7, JUNE 10-15, 2018 Waikoloa, Hawaii
- [10] R. King, D. Bhusari, A. Boca, D. Larrabee, X.-Q. Liu, W. Hong, C. Fetzer, D. Law, N. Karam, "Band gap-voltage offset and energy production in next-generation multijunction solar cells," *Progress. Photovolt: Res. Appl.* 19 (7) (2011) 797–812.
- [11] K. Tanabe, D. Guimard, D. Bordel, Y. Arakawa, "High-efficiency InAs/GaAs quantum dot solar cells by metalorganic chemical vapor deposition," *Appl. Phys. Lett.* 100 (2012) (1293905-193905-3).
- [12] Aho, T., Guina, M., Elsehrawy, F., Cappelluti, F., Raappana, M., Tukiainen, A., ... & Niemi, T. (2018). Comparison of metal/polymer back reflectors with half-sphere, blazed, and pyramid gratings for light trapping in III-V solar cells. *Optics express*, 26(6), A331-A340.
- [13] A. Luque and A. Martí, "Increasing the efficiency of ideal solar cells by photon induced transitions at intermediate levels," *Phys. Rev. Lett.* 78, 5014-5017 (1997).